Anti-glioblastoma Effects of Structural Variants of Benzoylphenoxyacetamide (BPA): II. Synthesis Strategies for Phenolic Variants of BPAs With Potential for Blood Brain Barrier Penetration.

Joanna Stalinska
Louisiana State University Health Sciences Center, Stanley S. Scott Cancer Center, Department of Interdisciplinary Medicine, New Orleans, LA 70112

Cecilia Vittori
Louisiana State University Health Sciences Center, Stanley S. Scott Cancer Center, Department of Interdisciplinary Medicine, New Orleans, LA 70112

Charles H. Ingraham IV
Louisiana State University Health Sciences Center, Stanley S. Scott Cancer Center, Department of Interdisciplinary Medicine, New Orleans, LA 70112

Sean C. Carson
University of New Orleans

Karlie Bonstaff
Louisiana State University Health Sciences Center, Stanley S. Scott Cancer Center, Department of Interdisciplinary Medicine, New Orleans, LA 70112

Adam Lassak
Louisiana State University Health Sciences Center, Stanley S. Scott Cancer Center, Department of Interdisciplinary Medicine, New Orleans, LA 70112

Celeste Faia
Louisiana State University Health Sciences Center, Stanley S. Scott Cancer Center, Department of Interdisciplinary Medicine, New Orleans, LA 70112

Susan B. Colley
Louisiana State University Health Sciences Center, Stanley S. Scott Cancer Center, Department of Interdisciplinary Medicine, New Orleans, LA 70112

Francesca Peruzzi
Louisiana State University Health Sciences Center, Stanley S. Scott Cancer Center, Department of Interdisciplinary Medicine, New Orleans, LA 70112

Krzysztof Reiss (kreiss@lsuhsc.edu)
Louisiana State University Health Sciences Center, Stanley S. Scott Cancer Center, Department of Interdisciplinary Medicine, New Orleans, LA 70112

Branko S. Jursic

Research Article

Keywords: temozolomide (TMZ), MPO-CNS, logS, blood-brain partitioning, surgical resection

Posted Date: September 21st, 2021

DOI: https://doi.org/10.21203/rs.3.rs-909472/v1

Anti-glioblastoma effects of structural variants of benzoylphenoxyacetamide (BPA): II. Synthesis strategies for phenolic variants of BPAs with potential for Blood Brain Barrier penetration.

Joanna Stalinska[c,d], Cecilia Vittori[c,e], Charles H. Ingraham IV[a], Sean C. Carson[a], Karlie Bonstaff[c], Adam Lassak[c], Celeste Faia[c], Susan B. Colley[c], Francesca Peruzzi[c], Krzysztof Reiss[c*], and Branko S. Jursic[a,b*]

[a]Department of Chemistry, University of New Orleans, New Orleans, LA 70148, United States; [b]Stepharm llc., PO Box 24220, New Orleans, LA 70184, United States; [c]Neurological Cancer Research, Stanley S. Scott Cancer Center, Department of Medicine, LSU Health Sciences Center, New Orleans, LA 70112; [d]Department of Cell Biology, Faculty of Biochemistry, Biophysics and Biotechnology, Jagiellonian University, Cracow Poland; [e]Department of Biomedical and Clinical Sciences L. Sacco, University of Milan, Milan, Italy.

*corresponding authors

ABSTRACT

Glioblastomas are the most aggressive brain tumors for which therapeutic options are limited. Current therapies against glioblastoma include surgical resection, followed by radiotherapy plus concomitant and maintenance with temozolomide (TMZ), however, these standard therapies are often ineffective, and average survival time for glioblastoma patients is between 12 and 18 months. We have previously reported a strong anti-glioblastoma activity of several metabolic compounds, which were synthetized based the chemical structure of a common lipid-lowering drug, fenofibrate, and share a general molecular skeleton of benzoylphenoxyacetamide (BPA). Extensive computational analyses of phenol and naphthol moieties added to the BPA skeleton were performed in this study with the objective of selecting new BPA variants for subsequent compound preparation and anti-glioblastoma testing. Initially, 81 structural variations were considered and their physical properties such as solubility (logS), blood-brain partitioning (logBB), and probability of entering the CNS calculated by the Central Nervous System – Multiparameter Optimization (MPO-CNS) algorithm were evaluated. From this initial list, 18 compounds were further evaluated for anti-glioblastoma activity *in vitro*. Nine compounds demonstrated desirable glioblastoma cell toxicity in cell culture, and two of them, HR51, and HR59 demonstrated significantly improved capability of crossing the model blood-brain-barrier (BBB) composed of endothelial cells, astrocytes and pericytes.

INTRODUCTION

Glioblastomas are the most aggressive brain tumors for which therapeutic options are very limited [1,2]. Current standard of care therapies include maximal surgical resection, followed by radiotherapy plus concomitant and maintenance with temozolomide (TMZ), however, these standard therapies are often ineffective, contributing to the dismal glioblastoma patient survival time of 12-18 months [3]. Multiple genetic and epigenetic abnormalities have been found in glioblastomas, among which p53, EGFR, PTEN, and IDH mutations are the most common [4-6]. In spite of these validated therapeutic targets, molecular, gene-therapy, and immunotherapy approaches are still ineffective [7,8]. Therefore, new and more effective therapies for glioblastoma patients are desperately needed.

There are several reasons why it is difficult to treat glioblastoma. **First**, glioblastomas are characterized by many dysregulated pathways that cannot be blocked simultaneously with a single therapy [9]; **Second**, glioblastomas are highly infiltrating and create heterogenous tumors that are very difficult to be removed by surgery without compromising the function of the surrounding brain areas [10]; **Third**, early diagnosis of glioblastoma is rare, therefore, large highly infiltrating and vascularized tumors are often already present at the time of diagnosis [11]. **Fourth**, the optimization of clinical protocols for glioblastoma treatment requires the use of a reliable preclinical model/s. Unfortunately, commonly used rodent syngeneic and xenograft models have one major problem - the experimental tumors are typically ~10^3-10^4 smaller than human tumors, and therefore, drug delivery, drug retention, and effective tissue penetration by the drug, cannot be tested in a reliable manner in small animal models [12]; **Fifth,** the blood brain barrier (BBB)

prevents the majority of anticancer drugs from reaching the tumor site, and current methods that enhance the BBB penetration are not effective for glioblastoma patients [13].

One of the drugs that readily crosses the BBB is temozolomide (TMZ). Upon oral administration, TMZ maximum plasma concentration can be reached in about one hour, and the elimination half-life is approximately 2.1 hours. Importantly, penetration efficiency of TMZ into the CNS is experimentally estimated to be about 20% of the plasma levels [14]. Applying this estimate to calculate the logBB (Brain-Blood Distribution) for TMZ, this equation produces a value of -0.7, which indicates sufficient capability of the compound to cross the BBB [15]. In spite of these positive features, TMZ-treated glioblastoma patients develop TMZ-resistance and recurrent tumors are practically incurable [16]. There are also several studies of the use of TMZ in combination with other drugs, which show beneficial therapeutic effects [17] [18]. One interesting example is a combination of TMZ with lipid lowering drugs, including statins [19]. In addition, another class of lipid-lowering compounds, fibrates, have also attracted attention as a possible anticancer drugs [20-23]. We have previously reported that 50μM fenofibrate (**FF)** has a strong anti-glioblastoma activity in cell culture, and in glioblastoma mouse models following intratumoral injection [24] (Scheme 1). However, **FF** does not cross the BBB, and is quickly processed by the blood and tissue esterases to form fenofibric acid (**FFA**), which is no longer effective in triggering tumor cell death [24,25].

We have previously made several chemical modifications to the **FF** molecular skeleton, to address the **FF** low stability in human blood, low water solubility, and inability of penetrating the BBB. Indeed, one of the initial compounds, **PP1,** demonstrated improved water solubility and stability in human blood. In addition, **PP1** was capable of

triggering extensive glioblastoma cell death *in vitro* at concentrations over 4-fold lower than **FF** [26] (Scheme 1)**.** To further improve anti-glioblastoma efficacy, we created other **FF** derivatives, which share the benzoyl-phenoxy-acetamide **(BPA)** molecular skeleton, and decided to test the addition of phenol and naphthol residues to the BPA structure due to the potential anti-cancer effects of these moieties [27-30]. As a result, 18 new compounds were generated and were analyzed during this study.

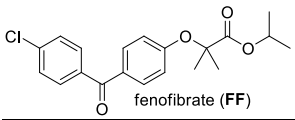

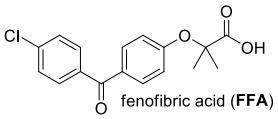

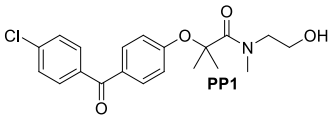

	FF	FFA	PP1
Water Solubility	Low	Moderate	Moderate
Resistance to blood esterases	Low	High	High
Antitumoral effect	IC50*= 31.83 μM	No	IC50*=7.7 μM

Scheme 1. *Comparison between **FF**, **FFA**, and **PP1** structural and anti-cancer properties. The information regarding the compounds water solubility, stability in human blood, and in vitro cytotoxicity were previously reported [31]. *determined using LN229 monolayer cultures and MTT assay.*

RESULTS and DISCUSSON

Overall Chemical Design: In our previous studies we have explored the importance of a basic **BPA** skeleton [31], and concluded that BPA could serve as a "pharmacophore", necessary to retain anti-glioblastoma activity [32,33]. The amide part of the **BPA** skeleton can be specifically modelled to obtain a more desirable anti-tumor activity. This includes, among other properties, chemical and physical parameters (described below) that contribute to the increased BBB penetration, and possibly drug retention within the tumor tissue. In this regard, we have selected phenol and naphthol residues due to mounting evidence supporting the role of different derivatives of these compounds in health benefits [34], including anti-cancer activities [28,29]. In this paper, three variants of **BPA** are discussed: a substituted phenol (***Phenolic-BPA***)], and two naphtholic BPAs (***1-Naphtholic-BPA*** and

2-Naphtholic-BPA) (Scheme 2) that serve as prototype molecules for further modifications.

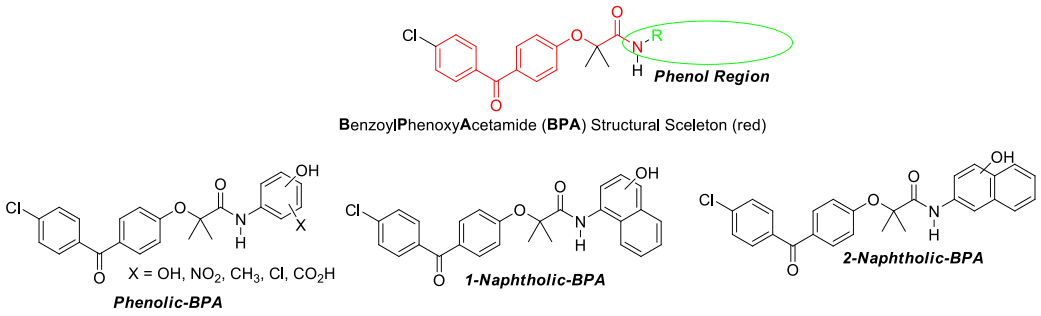

Scheme 2. *Phenol region of* ***BPA*** *skeleton selected for modification (circle) in search of the optimal anti-glioblastoma drug.*

The starting point for the preparation of all phenolic **BPAs** is fenofibric acid (**FFA**), and the corresponding aminophenol or aminonaphthol residues (Scheme 3) are added through amide (peptide) coupling reactions [35,36]. As previously reported [31], due to the steric hindrance of the carboxylic group of **FFA**, which includes two methyl groups in the alpha position of carboxylic acid, combined with the lower amine nucleophilicity of anilines in DCC- or EDC-coupling, these reactions do not produce acceptable isolated yields. This occurs even with more reactive aminophenols and EDC or DCC, which are stronger nucleophiles compared to nonactivated anilines, which is expected to produce corresponding **BPA** compounds in acceptable yields [37]. However, we were able to detect only traces of the desirable products with these methods, and instead, decided to convert **FFA** into the more reactive fenofibrate chloride (**FFC**), followed by coupling with aminophenols or aminonaphthols (Scheme 3). We have explored several variations of this procedure and finally selected one that is very simple and can be applied to multigram and even multikilogram production scales. In particular, the **FFC** was prepared fresh and immediately used, for the next step of aminophenol addition (Scheme 3). The most

common method of preparation of an acid chloride is by using thionyl chloride. This requires heating of thionyl chloride with the corresponding acid (in this case **FFA**) with appropriate traps for hydrochloric acid and sulfur dioxide, which are undesirable biproducts of the reaction [38].

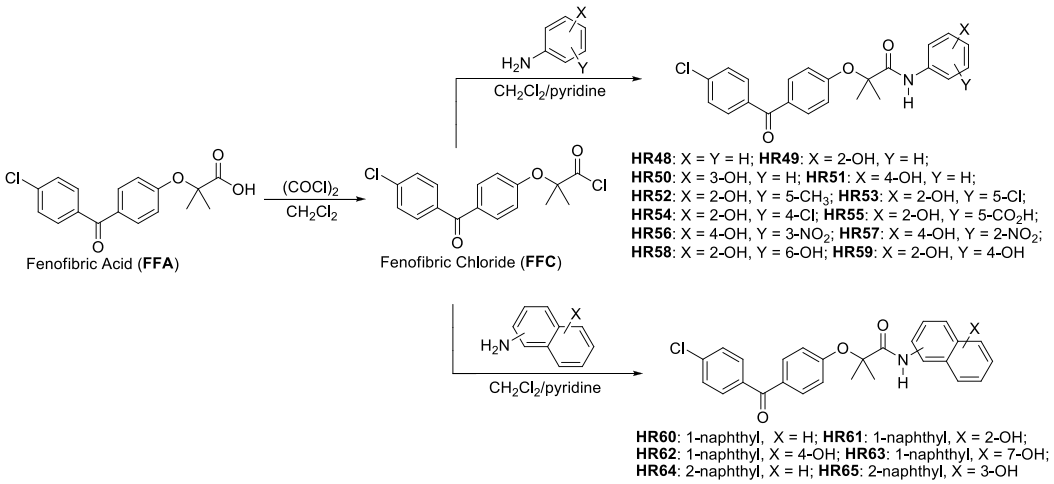

Scheme 3. *Schematic illustration of the procedure for preparation of hydroxylated phenyl and naphthyl derivatives of BPA.*

Biological, Chemical and Computational Testing of the Compounds: Previously, we have reported that some amide derivatives of **FF**, including **PP1**, are more potent than others in eliminating glioblastoma cells [26] and belong to the large family of **BPA** [39]. Further modifications of the **BPA** structure were designed to produce compounds with the improved ability to penetrate BBB, and superior glioblastoma cytotoxicity. This is highly relevant for glioblastoma patients, since one fundamental challenge for new drug development is the need for effective BBB penetration. So far, known BBB-permeable compounds form a very small subset of current oral drugs, and experimental models for testing BBB penetration by new drugs are complex and expensive. Therefore, an independent indicator of the BBB penetration is necessary for faster and more cost effective analyses of new anti-glioblastoma drug candidates. This is critical for the initial

screening of a large number of compounds, including **BPA** variants, and selection of best candidates for subsequent measurements of intracranial tumor drug penetration and anti-tumoral efficacy.

Therefore, we performed extensive molecular modeling prior to preparation of new **BPA** variants in order to evaluate their specific physicochemical properties considered relevant for the BBB penetration. We have applied first a weighted scoring approach named "Central Nervous System – Multiparameter Optimization" (CNS-MPO) [40,41]. The CNS-MPO algorithm uses 6 key physicochemical properties (clogP, clogD, MW, TPSA, HBD, and pKa) with the scores ranging between 0 and 6.0. Importantly, scores ≥ 4.0 are widely accepted for selecting compounds with high potential for CNS penetration [41]. The validation of this approach was based on a library of 616 compounds for which experimental distribution of the drug in CNS was determined and the corresponding parameters of the compound incorporated into CNS-MPO scores [40,41]. It was found that CNS-MPO scores of 1-2 (0%), 2-3 (11.6%), 3-4 (40.8%), 4-5 (53.8 %) and 5-6 (81.1%) correlated with the increased probability of drugs to be found in the brain [42].

In addition to CNS-MPO, other chemical and physical parameters of the Quantitative Structure Activity Relationship (QSAR) studies were also used in our calculations to further increase the probability of BBB penetration by the compound. These include: molecular polarizability (MP), minimal molecular projection area (MPA), water solubility (LogS), and lipophilicity (cLogP) to name a few. These parameters are not incorporated in the CNS-MPO score, however, they also play a role in the estimation of compound ability to penetrate the BBB [43]. Therefore, we have calculated and incorporated all these additional parameters when evaluating and selecting new HR compounds as

potential anti-glioblastoma drugs (Figs. 1-6; and supplementary materials). In particular, MP is a response of electron distribution to an externally-applied static electrical field. Comparing MP values helps in understanding how different substrates may change polarization- and dispersion-type during interactions with the active sites of their interacting proteins [44]. It was postulated that MP values between 30-40 (see supplementary data) are optimal for a molecule to bind to a biotarget [45]. Minimal projected area (MPA) represents another parameter that is important for drug transport and ultimately for drug activity. For instance, a distinct phenotypical pattern of drug recognition and transport for the G616N variant was reported, indicating that drug substrates with MPA over 70 $Å^2$ are less likely to be transported compared to drugs with smaller MPA [46]. In addition, LogS of -4.5 and greater are indicators of acceptable water solubility [47], and the rate of passive diffusion is inversely proportionate to the square root of molecular size (Graham's law [48]), which are also included in our compound analysis.

Finally, the ability of the compound to penetrate the BBB can also be expressed as a decimal logarithm of brain to plasma concentration ratio (logBB), which is derived from the modified Clark's equation: logBB =0.152 ClogP-0.0148PSA + 0.139 30. It has been shown that compounds with logBB > 0.3 readily cross the BBB, while the compounds with logBB < - 1.0 have a problem with the CNS penetration [15]. Therefore, LogBB values for all HR compounds were also calculated and included (Figs. 1-5).

Once all above calculations were performed, initial cell viability (CV) tests were performed for all HR compounds using LN229 human glioblastoma cell line. The cells were treated with proposed HR compounds at 25 μM, and cell viability was evaluated

using MTT assay, following a continuous cell exposure to a single dose of the drugs for 72 hrs. (Figs. 1-6).

As a result of this initial screening, we have identified two lead drug candidates, **HR51** and **HR59**, with phenolic moieties that contain BPA structural skeleton similar to our prototype anti-glioblastoma compound PP1 [26]. This is in addition to our recently reported BPA-based compounds (HR28, HR32, HR37, and HR46), which also demonstrated high potential as anti-glioblastoma drugs [31]. Anti-glioblastoma effects of HR51 and HR59 were subsequently confirmed using four different human glioblastoma cell lines, LN229, U-87 MG, U-118 MG, T98G, and the cytotoxicity data were compared to normal human astrocytes (NHA). Results in Fig. 6A demonstrate that all tested glioblastoma cells were partially responsive to 10μM HR51 and HR59, but were almost completely eliminated following 72 hour exposure to 25μM HR51 or HR59. In contrast, these two compounds were significantly less cytotoxic to normal human astrocytes (NHA), indicating that these two new compounds may have low CNS toxicity. In addition, results in Fig. 6B show that IC_{50} concentrations for HR51 and HR59 are below 10 μM, which is an acceptable therapeutic concentration for clinically relevant anticancer drugs.

We have also tested if the mechanism of action of HR51 and HR59 is similar to our prototype drugs, PP1 and fenofibrate, which have been previously shown to inhibit mitochondrial respiration at the level of Complex 1 of the electron transport chain (ETC)[24,26]. Indeed, results in Fig. 6C confirmed that both HR51 and HR59 inhibit mitochondrial respiration in the magnitude similar to PP1.

In addition to a strong *in vitro* anti-glioblastoma activity (Fig. 6), HR51 and HR59 have physical properties that may contribute to the improved brain tumor penetration. Specifically, HR51 and HR59, have a minimal projection area (MPA) of 46.23 $Å^2$ and 43.73 $Å^2$ [46], respectively; water solubility (LogS) of -6.61 and -6.11 [47]; and brain to plasma concentration ratio (LogBB) of -0.15 and -0.49 [15], which are all considered as highly promising for compounds suspected of being capable of penetrating the brain tumor tissue.

Importantly, HR51 and HR59 can also cross the triple-coculture model of the blood brain barrier (BBB), which consists of astrocytes, pericytes and epithelial cells cultured on 24-well (3μm pores) transwell membranes (Fig. 7A), prepared according to the protocol provided by Stone et al. [49]. All experiments in which the ability of HR compounds to cross the BBB were evaluated using the BBB inserts that demonstrated a significant increase of the electric resistance (Ω) in comparison to inserts without cells ($\Omega_{BBB} - \Omega_{Insert}$) (Fig. 7B). In particular, $\Omega_{BBB} - \Omega_{Insert}$ values of 105.3+/-16; 110.6+/-14; 117.8 +/-19; 132.3 +/-23; and 129.0+/-24 were measured for inserts used to evaluate BBB penetration of FF, caffeine, HR51 and HR59, respectively (Fig. 7B). Accordingly, trans-endothelial electric resistance (TEER = $\Omega_{BBB} - \Omega_{Insert}$ x area of the membrane)[49,50] for the inserts used for FF, caffeine, HR51 and HR59 testing are: 34.7+/-5.3; 36.5+/-4.6; 43.7+/-7.6; and 42.6+/-8.1, respectively. These TEER values are comparable to TEER values obtained from similar triple-coculture model of the BBB in which 24-well inserts with 3μm pores were previously evaluated [49], indicating effective electric resistance produced by our BBB model.

Following TEER measurements, 25μM HR51, 25μM HR59, as well as 50μM caffeine (positive control [51]) and 25μM fenofibrate (negative control [25]) were added to the corresponding insert and the plates were incubated in 37^0C and 5% CO_2 for 24 hrs. Subsequently, aliquots of media from the corresponding inserts and from the wells were collected for HPLC measurements and to calculate BBB permeability ($P=V_A \cdot C_A/(t \cdot S \cdot C_L)$ [52]. Results in Fig. 7C show that HR51, HR59 and caffeine cross the *in vitro* BBB at levels 4.4-fold, 3.5-fold and 22.0-fold higher compared to our internal negative control, fenofibrate, which although has a similar molecular weight and structure to the tested HR compounds (Fig. 1), its ability of crossing natural BBB is very low [25].

By exploring the computed structural variations of phenolic-**BPA**s, and testing their cell toxicity, we have demonstrated that the addition of phenol moieties improves anti-glioblastoma activity with acceptable LogBB and LogS properties. This could be further improved by adding additional substituent(s) to the phenol moiety, including hydroxy group, halogen, alkyl, nitro on carbonyl to name a few. However, replacing the phenol residue with the larger naphthol, although it might not compromise anti-glioblastoma activity in cell culture, it may result in decreased compound bioavailability mostly due to low water solubility (Fig. 4) [53]. Therefore, these naphthol compounds are less likely to be considered as anti-glioblastoma candidates. Further exploration of phenolic BPAs, using proposed algorithms in combination with the *in vitro* BBB penetration model, represents a quick, reliable and relatively inexpensive way of testing a large number of new drug candidates in the preparation for extensive pharmacokinetic and efficacy testing in empirical animal models.

A

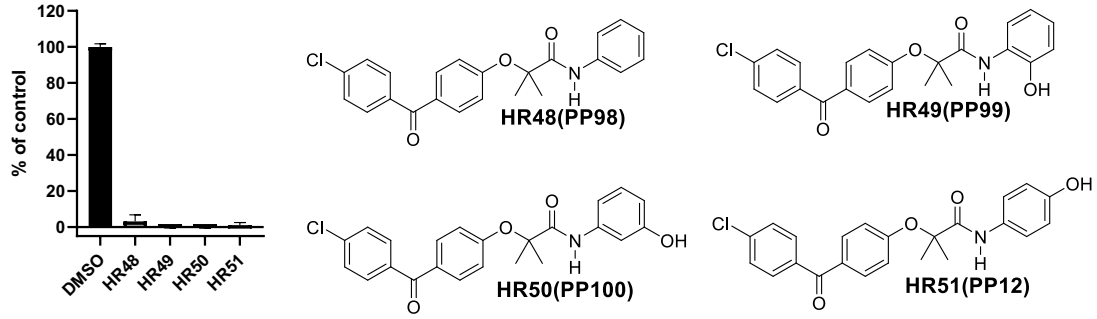

B

Comp.	CV	MW	Clog P	HB D	HBA	PSA	MPA	logBB	LogS	MPO
HR48	3.19 ± 3.64	393.86	5.79	1	3	55.40	43.73	0.20	-7.07	2.59
HR49	0 ± 0.27	409.86	5.49	2	4	75.63	48.14	-0.15	-6.61	2.76
HR50	0 ± 0.48	409.86	5.49	2	4	75.63	43.83	-0.15	-6.61	2.50
HR51	1.1 ± 1.42	409.86	5.49	2	4	75.63	46.23	-0.15	-6.61	2.45

C

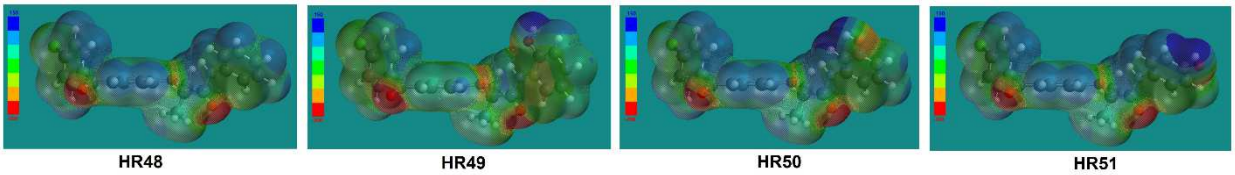

D

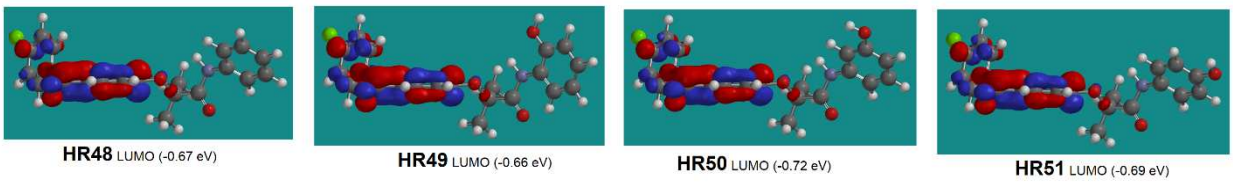

E

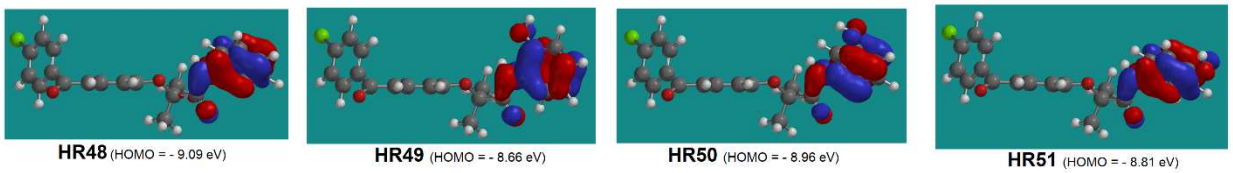

Figure 1. *<u>Drug candidates with hydroxy substituted phenylamide moiety.</u>* ***Panel A:*** *Cell viability (MTT assay) following exposure to modified variants of* ***HR48*** *with one hydroxy groups in different positions in the phenylamide moiety (25 μM, for 72 hrs).* ***Panel B:*** *CV = Cell viability (% of control) mean ± SD at 25 μM; ClogP = calculated partitioning; HBD = hydrogen bond donor at pH = 7; HBA = hydrogen bond acceptor at pH =7; logBB = calculated blood-brain partition; PSA = Polar surface area (Å^2); MPA = Minimal projection area (Å^2); LogS = Aqueous solubility (mg/ml); MPO = Central nervous system multiparameter optimization (CNS MPO).* ***Panel C:*** *Electrostatic potential map for* ***H48-HR51****.* ***Panel D:*** *Computed LUMO orbitals contribution with their energies.* ***Panel E:*** *Computed HOMO orbitals contribution with their energies generated by semi-empirical method PM3 as implemented in Spartan '18 version 1.1.0*

A

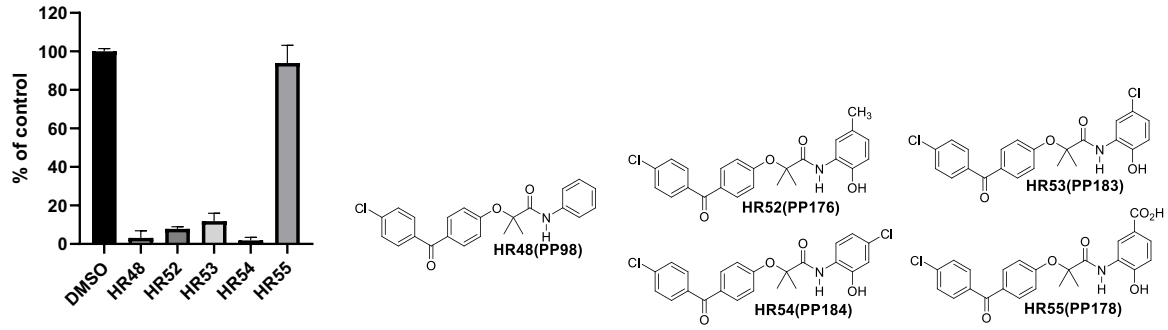

B

Comp.	CV	MW	ClogP	HBD	HBA	PSA	MPA	logBB	LogS	MPO
HR48	3.19 ± 3.64	393.86	5.79	1	3	55.40	43.73	0.20	-7.07	2.59
HR52	7.81 ± 1.12	423.89	6.00	2	4	75.63	48.18	-0.07	-7.09	2.49
HR53	11.81 ± 4.17	444.31	6.09	2	4	75.63	49.87	-0.05	-7.10	2.79
HR54	1.89 ± 1.56	444.31	6.09	2	4	75.63	46.41	-0.05	-7.08	2.90
HR55	93.95 ± 9.16	453.87	5.15	3	6	112.93	52.16	-0.75	-3.20	2.72

C

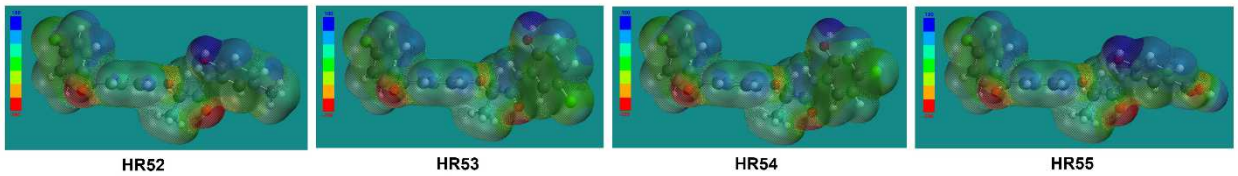

D

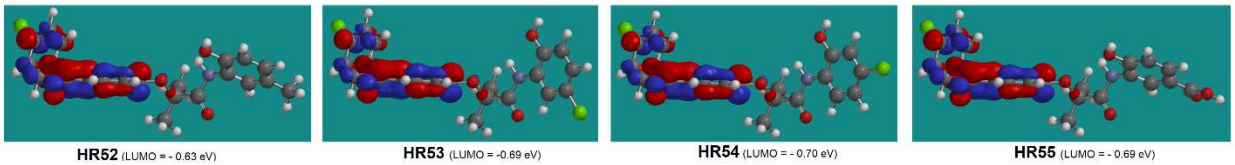

E

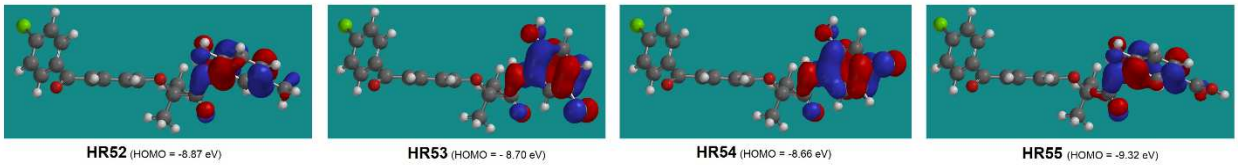

Figure 2. *<u>Drug candidates with sutituted 2-hydroxyphenylamide moiety.</u>* ***Panel A:*** *Cell viability (MTT assay) following exposure to modified variants of* ***HR48*** *with ortho hydroxy and ether methyl, chloro, or carboxy group in the phenylamide moiety (25 μM, for 72 hrs).* ***Panel B:*** *CV = Cell viability (% of control) mean ± SD at 25 μM; ClogP = calculated partitioning; HBD = hydrogen bond donor at pH = 7; HBA = hydrogen bond acceptor at pH =7; logBB = calculated blood-brain partition; PSA = Polar surface area (Å²); MPA = Minimal projection area (Å²); LogS = Aqueous solubility (mg/ml); MPO = Central nervous system multiparameter optimization (CNS MPO).).* ***Panel C:*** *Electrostatic potential map for* ***H52-HR55****.* ***Panel D:*** *Computed LUMO orbitals contribution with their energies.* ***Panel E:*** *Computed HOMO orbitals contribution with their energies generated by semi-empirical method PM3 as implemented in Spartan '18 version 1.1.0*

A

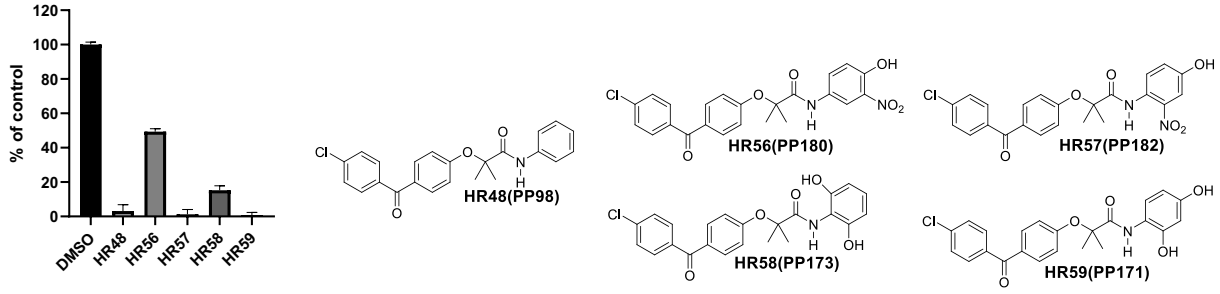

B

Comp.	CV	MW	ClogP	HBD	HBA	PSA	MPA	logBB	LogS	MPO
HR48	3.19 ± 3.64	393.86	5.79	1	3	55.40	43.73	0.20	-7.07	2.59
HR56	49.36 ± 1.67	454.86	5.43	2	6	118.77	47.89	-0.79	-6.50	1.86
HR57	1.29 ± 2.79	454.86	5.43	2	6	118.77	47.50	-0.79	-7.05	1.86
HR58	15.22 ± 2.61	425.86	5.19	3	5	95.86	49.54	-0.49	-6.10	2.21
HR59	0.88 ± 1.5	425.86	5.19	3	5	95.86	47.89	-0.49	-6.11	2.16

C

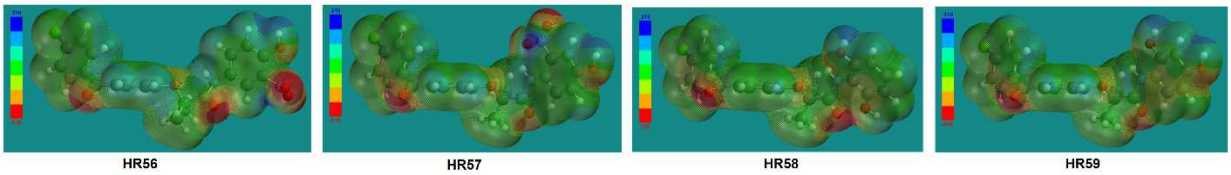

D

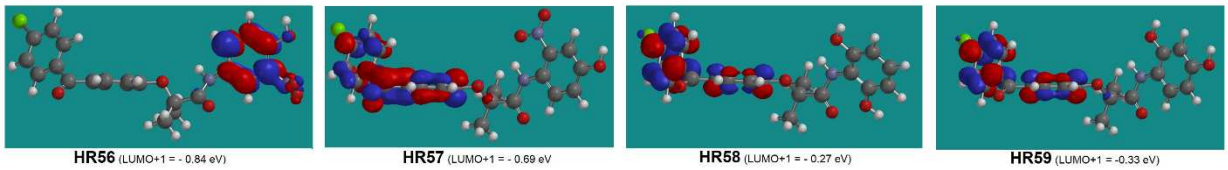

E

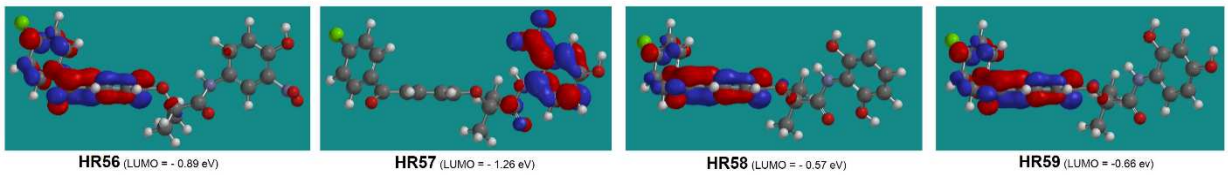

F

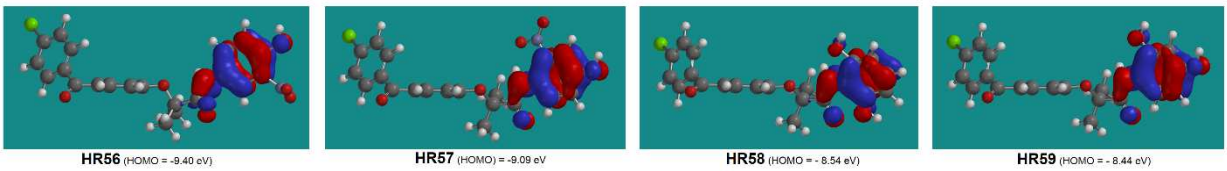

Figure 3. *Drug candidates with nitro-hydroxy and two hydroxy sutituted phenylamide moiety.* ***Panel A:*** *Cell viability (MTT assay) following exposure to modified variants of* ***HR48*** *with one hydroxy and one nitro group or with two hydroxy groups in the phenylamide moiety (25 μM, for 72 hrs).* ***Panel B:*** *CV = Cell viability (% of control) mean ± SD at 25 μM; ClogP = calculated partitioning; HBD = hydrogen bond donor at pH = 7; HBA = hydrogen bond acceptor at pH =7; logBB = calculated blood-brain partition; PSA = Polar surface area (Å²); MPA = Minimal projection area (Å²); logS = Aqueous solubility (mg/ml); MPO = Central nervous system multiparameter optimization (CNS MPO).* ***Panel C:*** *Electrostatic potential map for* ***H56-HR59****.*

Panel D: *Computed LUMO+1 orbitals contribution with their energies.* ***Panel E:*** *Computed LUMO orbitals contribution with their energies.* ***Panel F:*** *Computed HOMO orbitals contribution with their energies generated by semi-empirical method PM3 as implemented in Spartan '18 version 1.1.0*

A

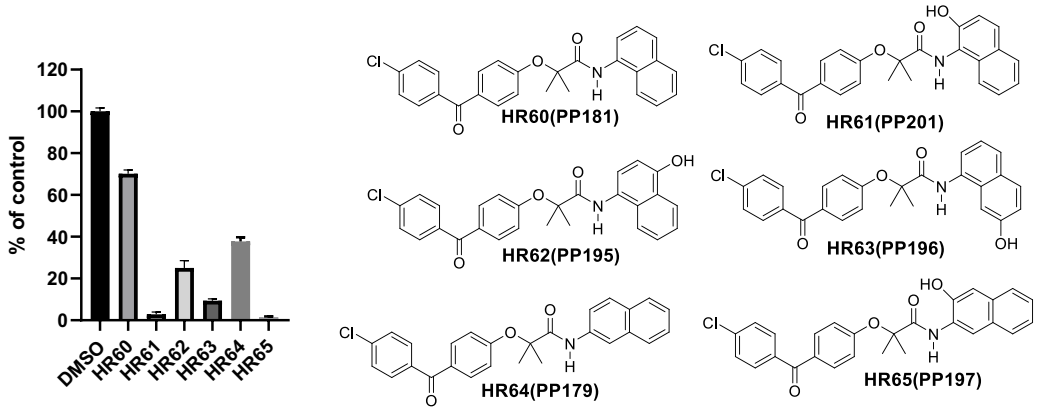

B.

Comp.	CV	MW	ClogP	HBD	HBA	PSA	MPA	logBB	LogS	MPO
HR60	70.13 ± 1.79	443.92	6.78	1	3	55.40	50.10	0.35	-8.79	2.23
HR61	2.87 ± 1.05	459.92	6.48	2	4	75.63	48.22	0.01	-8.28	2.51
HR62	25.03 ± 3.56	459.92	6.48	2	4	75.63	50.50	0.01	-8.33	2.26
HR63	9.33 ± 0.88	459.92	6.48	2	4	75.63	53.68	0.01	-8.33	1.93
HR64	37.7 ± 2.03	443.92	6.78	1	3	55.40	50.72	0.35	-8.79	2.23
HR65	1.49 ± 0.32	459.92	6.48	2	4	75.63	50.52	0.01	-8.29	2.53

C

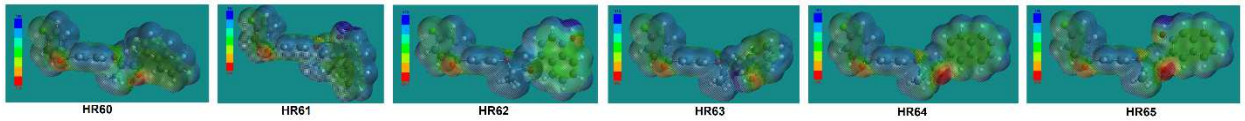

D

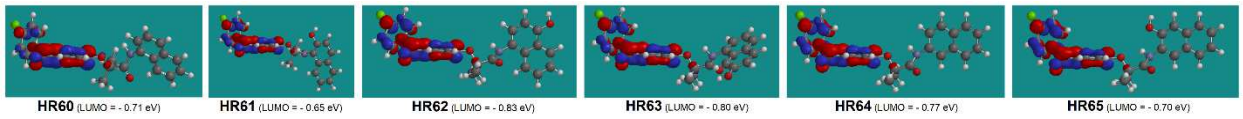

E

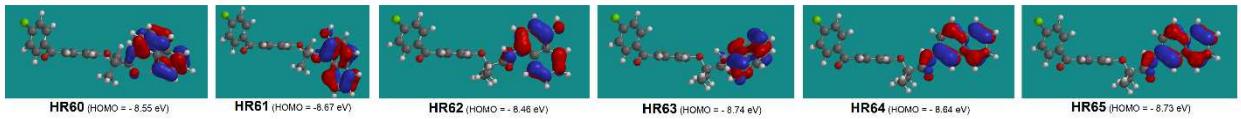

Figure 4. *<u>Drug candidates with hydroxy substituted naphthylamide moiety.</u>* ***Panel A:*** *Cell viability (MTT assay) following exposure to modified variants of 1- and 2-naphthylamide of* ***HR60*** *and* ***HR64*** *with one hydroxy group in the naphthylamide moiety (25 μM, for 72 hrs).* ***Panel B:*** *CV = Cell viability (% of control) mean ± SD at 25 μM; ClogP = calculated partitioning; HBD = hydrogen bond donor at pH = 7; HBA = hydrogen bond acceptor at pH =7; logBB = calculated blood-brain partition; PSA = Polar surface area (Å^2); MPA = Minimal projection area (Å^2); logS = Aqueous solubility (mg/ml); MPO = Central nervous system multiparameter optimization (CNS MPO).* ***Panel C:*** *Electrostatic potential map for* ***H60-HR65****.* ***Panel D:*** *Computed LUMO orbitals contribution with their energies.* ***Panel E:*** *Computed HOMO orbitals contribution with their energies generated by semi-empirical method PM3 as implemented in Spartan '18 version 1.1.0.*

Comp.	logP	PSA	D+A	M1LogBB	M2LogBB	M3LogBB	M4LogBB	logS	CNS-MPO
PP1	3.31	66.84	5	-0.49	-0.35	0.01	-1.91	-5.09	3.97
HR48	5.79	55.40	4	1.11	0.20	0.51	-0.41	-7.07	2.59
HR49	5.49	75.63	6	0.39	-0.15	0.26	-2.27	-6.61	2.76
HR50	5.49	75.63	6	0.39	-0.15	0.26	-2.27	-6.61	2.50
HR51	5.49	75.63	6	0.39	-0.15	0.26	-2.27	-6.61	2.45
HR52	6.00	75.63	6	0.65	-0.07	0.34	-2.15	-7.09	2.49
HR53	6.09	75.63	6	0.70	-0.06	0.35	-2.13	-7.10	2.79
HR54	6.09	75.63	6	0.70	-0.06	0.35	-2.13	-7.08	2.90
HR55	5.15	112.93	9	-0.81	-0.75	-0.17	-5.26	-3.20	2.74
HR56	5.43	118.77	8	-0.83	-0.80	-0.18	-4.82	-6.50	1.89
HR57	5.43	118.77	8	-0.83	-0.80	-0.18	-4.82	-7.05	1.86
HR58	5.19	95.86	8	-0.32	-0.49	0.01	-4.13	-6.10	2.21
HR59	5.19	95.86	8	-0.32	-0.49	0.01	-4.13	-6.11	2.16
HR60	6.78	55.40	4	1.62	0.35	0.66	-0.18	-8.79	2.23
HR61	6.48	75.63	6	0.90	0.002	0.41	-2.04	-8.28	2.51
HR62	6.48	75.63	6	0.90	0.002	0.41	-2.04	-8.33	2.26
HR63	6.48	75.63	6	0.90	0.002	0.41	-2.04	-8.33	1.93
HR64	6.78	55.40	4	1.62	0.35	0.66	-0.18	-8.79	2.23
HR65	6.48	76.63	6	0.87	-0.01	0.40	-2.08	-8.29	2.53

Figure 5. *Compiled three variation of computing logBB and estimated MPO-CNS values for HR48 - HR65. logP computed partition, PSA = computed polar surface area; ClogP = calculated partitioning; PSA = Polar surface area (Å^2); D = hydrogen bond donor at pH = 7; A = hydrogen bond acceptor at pH =7; MPO = Central nervous system multiparameter optimization (CNS MPO).*
M1LogBB = 0.5159 × log P − 0.0277×PSA−0.3462. For log BB≥0.3 [15].
M2logBB = 0.152logP - 0.0148PSA + 0.139. (Clark's model).
M3logBB = 0.155 x logP - 0.01 x PSA +0.164. (Rishton's model).
M4log BB = 0.2289 × log P − 0.0326 × PSA − 0.5671 × (D + A) + 2.3420. For log BB≥−1 [15].

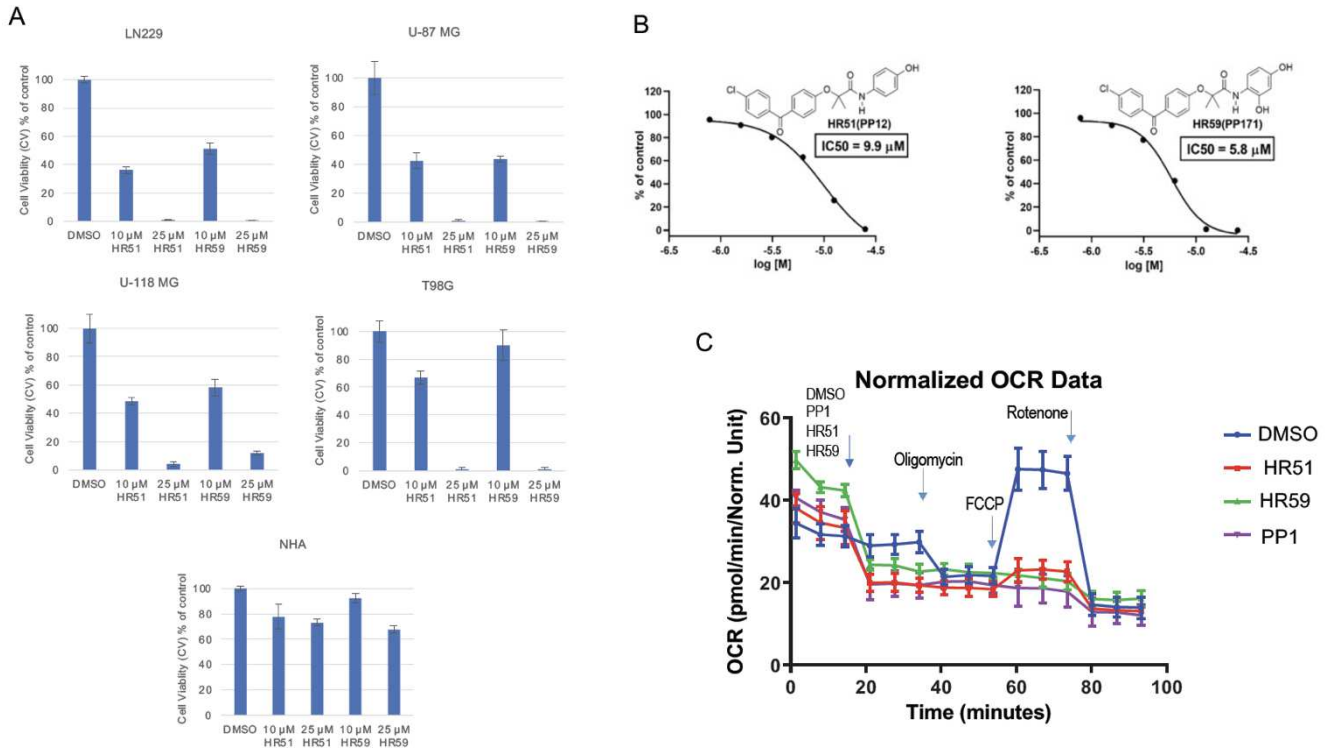

Figure 6. *<u>Cytotoxic effects of selected HR compounds.</u>* ***Panel A:*** *Effects of 10 and 25µM of HR51 and HR59 on the survival of human glioblastoma cell lines, LN229, U-87MG, U-118 MG, and T98G, compared to the effects of these two compounds on the survival of normal human astrocytes (NHA; LONZA/Clonetics™). Data were collected after 72 hours of a continuous cell exposure to a single dose of HR51 or HR59 in the low glucose medium (1g/L). Cells treated with DMSO (vehicle) were used as control. Data are expressed as cell viability (MTT, % of control) and represent average values with standard deviation (n=3).* ***Panel B:*** *Dose response curves and correlating IC50 values calculated for two most promising HR compounds, HR51 and HR59. Cell viability was evaluated by the MTT assay performed after exposure of LN229 to HR51 and HR59 for 72 hrs. Data represent mean values +/- SD (n=3).* ***Panel C:*** *<u>Metabolic effects of HR51 and HR59 compared to the prototype drug, PP1.</u> Metabolic responses to the drugs were evaluated in LN229 using Extracellular Flux Analyzer XF96 (Seahorse/Agilent). The oxygen consumption rate (OCR; indicative of mitochondrial respiration) was evaluated after injecting DMSO, (negative control), PP1 (positive control) and two experimental drugs, HR51 and HR59, followed by sequential injections of oilgomycin, FCCP; and rotenone (mitochondrial stress assay). Average OCR data were calculated from three independent experiments. Data represent average values +/- SD. Compared to negative control (DMSO), all tested metabolic compounds (PP1, HR51 and HR59) triggered an immediate drop in OCR. In addition, the cells treated with these three compounds did not respond to FCCP injection, indicating loss of the proton gradient across the mitochondrial membrane.*

A

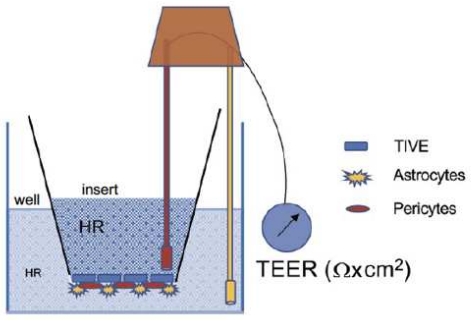

B

	Fenofibrate (FF)	Caffeine	HR49	HR51	HR59
TEER (Ω x cm²)	34.76 +/- 5.3 (n=3)	36.52 +/- 4.6 (n=3)	38.9 +/- 6.4 (n=3)	43.7 +/- 7.6 (n=3)	42.6 +/- 8.1 (n=3)
TEER coefficient*	0.95	1	1.06	1.2	1.17
$\Omega_{BBB} - \Omega_{insert}$	105.3 +/- 16 n=3	110.6 +/- 14 n=3	117.8 +/- 19 n=6	132.3 +/- 23 n=6	129.0 +/- 24 n=6

*fold change over Caffeine

C

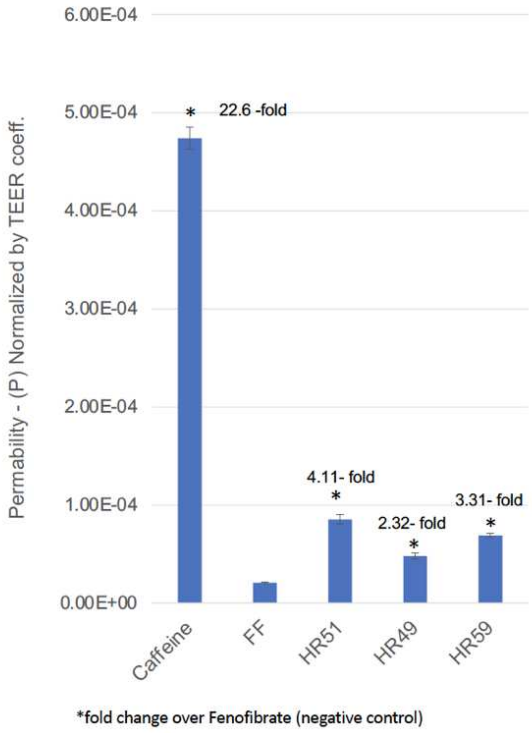

Figure 7: *<u>Penetration of the selected HR compounds through in vitro BBB model membrane:</u>* ***Panel A:*** *Schematic representation of a triple-coculture model of the BBB, which consists of astrocytes, pericytes and epithelial cells cultured on 24-well transwell membranes with 3μm pores. Trans-endothelial electric resistance (TEER) was measured using a EVOM^2 meter with a STX3 electrode (World Precision Instruments).* ***Panel B:*** *Measurements of the electric resistance of inserts used for specific compounds (Ω); Difference between resistance of the insert with established BBB versus empty insert ($\Omega_{BBB} - \Omega_{insert}$); and trans-endothelial electric resistance (TEER; $\Omega_{BBB} - \Omega_{insert}$ / cm^2). * TEER coefficient = TEER $_{compound}$ / TEER $_{caffeine}$. TEER coefficients were used to normalize BBB permeability (P) values to compensate for differences in TEER values between inserts selected for each compound.* ***Panel C:*** *Differences in BBB permeability (P) calculated using $P=V_A \cdot C_A/(t \cdot S \cdot C_L)$ equation [52] and normalized by TEER coefficient. Data represent average values from 2 independent experiments in triplicates (n=6) with standard deviation SD. * indicates values significantly different from fenofibrate (internal negative control).*

METHODS

All starting materials were reagent grade and purchased from Sigma–Aldrich, ArkPharm, and TCI America. ^{1}H-NMR spectra were recorded on Varian Mercury 300 and Varian Mercury 400 Plus instruments in $CDCl_3$ and DMSO-d_6, using the solvent chemical shifts as an internal standard [31]. All computed molecular descriptors were generated by ChemAxon MarvinSketch version 19.20. Electrostatic potential maps were calculated with a PM3 semi-empirical method as implemented in Spartan '18 v 1.1.0 [31]. ^{1}H-NMR and ^{13}C-NMR spectra for all HR compounds generated in this study are included in Supplementary Materials.

Method A (Larger scale preparation without extraction or crystallization). 2-(4-(4-chlorobenzoyl)phenoxy)-N-(2-hydroxyphenyl)-2-methylpropanamide (**HR49**). Fenofibric chloride (**FFC**) was freshly prepared from **FFA** (4.8 g; 0.015 mol) and oxalyl chloride (2.6 ml; 3.8g; 0.03 mmol). After drying with Argon, **FFC** was dissolved in dichloromethane (30 ml) and mixed with a pyridine (50 ml) solution of 2-aminophenol (1.3 g; 0.012 mol). The resulting solution was stirred at room temperature for 3 hours, and then at 70°C for an additional 3 hours with distillation of dichloromethane. The pyridine was removed under reduced pressure. The resulting solid substance was mixed with ethanol (50 ml) and the resulting mixture was refluxed by stirring until all of the solid was dissolved. This resulting clear alcohol solution was mixed with 3% sodium carbonate solution (300 ml) and heated with stirring at 80°C for one hour. After cooling to room temperature, the insoluble product was separated by filtration, extensively washed with water (10x100 ml) and dried at 110°C for 1 hour. The isolated yield was 97% (4.77 g). ^{1}H-NMR (DMSO-d_6, 400 MHz) δ 9.95 (1H, s, OH), 9.09 (1H, s, NH), 7.93 (1H, d, J = 8.0 Hz), 7.73 (2H, d, J = 8.0 Hz), 7.70 (2H,

d, J = 8.4 Hz), 7.59 (2H, d, J = 8.4 Hz), 7.11 (2H, d, J = 8.4 Hz), 6.23 (1H, t, J = 7.6 Hz), 6.83 (1H, d, J = 8.0 Hz), 6.78 (1H, t, J = 8.0 Hz), and 1.60 (6H, s) ppm. ^{13}C-NMR (DMSO-d_6) δ 193.8, 171.7, 158.9, 147.7, 137.6, 136.5, 132.2, 131.7, 131.3, 129.1, 126.1, 125.1, 121.2, 119.9, 119.6, 115.5, 82.3 and 25.3 ppm.

Method B (small scale preparation). Preparation of 2-(4-(4-chlorobenzoyl)phenoxy)-N-(2-hydroxy-5-methylphenyl)-2-methylpropanamide (**HR52**). A dichloromethane (10 ml) suspension of fenofibric acid (**FFA**) (191 mg; 0.6 mmol) and oxalyl chloride (0.2 ml; 384 mg; 2 mmol) was stirred at room temperature for five minutes. A few drops of *N*,*N*-dimethylformamide (DMF) were then added to the suspension, which induced bubbling, and resulted in a clear reaction mixture after approximately 30 minutes. This solution was then stirred at 60°C to promote slow solvent evaporation. The solvent residue and oxalyl chloride were removed by drying under an Argon flow at room temperature. The resulting yellow solid substance was dissolved in dichloromethane (10 ml) and mixed with 2-amino-4-methylphenol (62 mg; 0.5 mmol) in THF (10 ml) and Na_2CO_3 (1.06 g; 10 mmol) in water (10 ml). The subsequent mixture was stirred at room temperature for five hours. The solvent was then evaporated under reduced pressure and the residue was mixed with dichloromethane (50 ml) and water (50 ml). This final mixture was sonicated at room temperature until all solid was dissolved. From this bilayer solution, the water layer was discarded, and the dichloromethane layer was washed with 5% Na_2CO_3 (3x50 ml), water (50 ml), 5% HCl (3x50 ml), water (50 ml) and dried over anhydrous Na_2CO_3. After solvent evaporation, the final product was purified by crystallization from dichloromethane (~3ml) and hexane (20 ml). The isolated yield was 90% (190 mg). ^{1}H-NMR (DMSO-d_6, 400 MHz) δ 9.74 (1H, broad s, OH), 9.06 (1H, s, NH), 7.81 (1H, s), 7.73 (2H, d, *J* = 8.8 Hz), 7.70

(2H, d, *J* = 8.8 Hz), 7.58 (2H, d, *J* = 8.8 Hz), 7.11 (2H, d, *J* = 8.4 Hz), 6.73 (2H, s), 2.18 (3H, s), and 1.60 (6H, s) ppm. ^{13}C-NMR (DMSO-d_6) δ 193.8, 171.6, 158.8, 145.4, 137.7, 136.5, 132.2, 131.7, 131.3, 129.1, 128.1, 125.9, 125.3, 121.5, 119.9, 115.2, 82.2, 25.3, and 20.9 ppm.

Cell culture and viability assays. All cell culture procedures used for HR compound testing were previously described [26,31]. Briefly, human glioblastoma cell line, LN-229 (ATCC# CRL-2611), U-87MG (ATCC# HTB-14), U-118 MG (ATCC# HTB-15) and T98G (ATCC# CRL-1690) were maintained as semi-confluent monolayer cultures in DMEM (1 g/L glucose; with sodium pyruvate and L-glutamine) supplemented with 100 U/ml penicillin, 100 μg/ml streptomycin, and 10% fetal bovine serum (FBS) at 37°C in a 5% CO_2 atmosphere. In addition, normal human astrocytes (NHA) were used to evaluate effects of the selected HR compounds may have on normal not transformed cells. NHA were cultured according to the manufacturer protocol (LONZA/Clonetics™). Prior to the treatment with HR compounds, the cells were plated in 96-well plates (BD Falcon) at the initial density of 2 x 10^4/well. Twenty-four hours after plating, stock solutions of the HR compounds were prepared in DMSO, diluted in cell culture medium, to the final concentration of 25μM, and added to the cells in triplicate for every experimental condition. For the vehicle control, DMSO was used at 0.5%. After 72h incubation, MTT assay (surrogate for cell viability) was performed according to our previous publications [31]. Briefly, following 1.5 h incubation with MTT, formazan crystals were dissolved in 5mM HCl in isopropanol and the absorbance read at 540 nm. Data represent mean values expressed as % cell viability of control (DMSO) ± SD. Phase contrast images of treated

cells were taken 72 hours after treatment with HR compounds with a BZ-X800 fluorescence microscope (Keyence) equipped with a 20x objective. The drug dose causing 50% inhibition in the MTT assay at 72 hour time point (half maximal inhibitory concentration - IC50) was calculated using GraphPad Prism 8.

In vitro model of the blood brain barrier (BBB). The blood brain barrier was re-created *in vitro* using a modified protocol provided by Stone *et al* [49]. Briefly, 24-well transwell inserts (Falcon, catalog number 353096) were coated with 10μg/cm^2 of Collagen Type IV from human placentas (Sigma) for 24 hrs at 4°C. Inserts were washed with sterile water and air-dried for 2 hrs. Next, the inserts were coated with 2μg/cm^2 poly-L-lysine (ScienCell) for 1 hr at 37°C, then washed twice with sterile H_20 and air-dried for 2 hrs. 1.57x10^5 primary human astrocytes (ScienCell) and 3.125x10^4 primary human pericytes (ScienCell) were resuspended in 25μl of astrocyte medium and pericyte medium (ScienCell), respectively, then combined in a 1:1 ratio for 50μl total volume. Dried, coated inserts were turned upside down such that the basolateral surface was exposed at the top, and 50μl of the cell mixture was added to the membrane, covered with the plate lid, and incubated for 2 hrs at 37°C to allow cell adherence. Any medium remaining on top of the membrane was carefully removed before returning inserts to their upright position with the apical surface facing upward as they were placed in a 24-well plate containing 500μl per well of astrocyte/pericyte medium (1:1). An additional 300 μL of medium was added to the apical compartment. Four days after plating, the apical compartment medium was removed, and 3.75x10^4 of telomerase-immortalized vain endothelial cells (TIVE; provided by Dr. Rolf Renne) in 50μl of TIVE medium [54] were added and incubated

for 5 hrs at 37°C to allow cell adherence, followed by the addition of an extra 250μl of TIVE medium. Half the volume of the corresponding media in the lower and upper compartment was replaced with fresh media every third day. Ten days after initial plating, trans-endothelial electric resistance (TEER) was measured using a EVOM^2 meter with a STX3 electrode (World Precision Instruments). The ability of selected HR compounds to pass through *in vitro* BBB was tested using inserts with effectively reconstructed BBB as confirmed by TEER [49,50].

HPLC detection of selected HR compounds: Following TEER measurement, the medium from apical compartment of the *in vitro* BBB model (Fig. 7A) was replaced with 350μL of fresh TIVE medium containing corresponding compounds [HR49 (PP99), HR51 (PP12), HR59 (PP171)] all used at 25mM. In addition, 25mM fenofibrate (FF), which does not cross the BBB [25] was used as negative control, and 50μM caffeine was used as a positive control [51]. Plates containing the inserts were returned to the incubator (37°C, 5% CO_2), and after 24 hrs of incubation conditioned media from basolateral (well) and apical (insert) compartments were collected and frozen for quantitative analyses by HPLC. 100μl aliquots of the collected samples were subsequently mixed with 100μl of 100% acetonitrile, samples were centrifuged at 16.000 rpm at 4°C for 10 min and supernatants collected for HPLC analyses using UltiMate 3000 system (Thermo Scientific) equipped with analytical YMCbasic, 3μm, 150 x 4.6 mm column (octyl silane C8; YMC America, Inc.). Isocratic elution of the compounds was performed using mobile phase composed of solvent A (50 mM acetic acid in dH_2O) and solvent B (acetonitrile) mixed at ratios predetermined for each compound (Table 1). All separations were carried out with sample

volume of 5µl at flow rate of 1 ml/min, at 20°C. Concentration of each compound was calculated using serial dilutions of the known concentration of the compound separated at the same run with experimental and control samples. After separation, integrated areas under the peak were used to prepare calibration curves and to determine concentration of the compounds.

Table1. Details of the HPLC method for selected HR compounds.

Compound	Method length [min]	Concentration solvent B [%]	Detection wavelength [nm]	Retention time [min]
Caffeine	5	25	272	2.54
Fenofibrate	10	70	288	5.84
HR51	6	60	260	4.3
HR59	5	60	262	3.92

Evaluation of metabolic parameters

Metabolic responses of human glioblastoma cells were evaluated with Extracellular Flux Analyzer XFe96 (Agilent Technologies). During the day prior to each assay the cells were plated at $2x10^4$ cells/well in Agilent Seahorse 96-well XF cell culture microplates with growth supporting media and incubated overnight. At the time of measurement, growth media were replaced with serum-free XF assay medium (Seahorse XF Base Medium supplemented with 1 mM sodium pyruvate, 2 mM glutamine, and 5.5 mM glucose) and cartridges equipped with oxygen-sensitive and pH-sensitive fluorescent probes were placed above the cells. The oxygen consumption rate (OCR; indicative of mitochondrial respiration) was evaluated after injecting HR compounds or PP1 (all used at 25 µM), or DMSO (0.1%; vehicle control). These initial injections were followed by sequential injections of metabolic toxins to execute mitochondrial stress assay: oligomycin (inhibitor of ATP synthase; 0.5 µM); carbonylcyanide-p-

trifluoromethoxyphenylhydrazone (FCCP; uncoupling factor; 0.5 μM), rotenone (inhibitor of mitochondrial complex I; 0.3 μM), and antimycin A (inhibitor of mitochondrial complex III; 0.3 μM).

References

1 Nakada, M. *et al.* Molecular targets of glioma invasion. *Cell Mol Life Sci* **64**, 458-478 (2007).

2 Terzis, A. J., Niclou, S. P., Rajcevic, U., Danzeisen, C. & Bjerkvig, R. Cell therapies for glioblastoma. *Expert opinion on biological therapy* **6**, 739-749 (2006).

3 Montemurro, N. Glioblastoma Multiforme and Genetic Mutations: The Issue Is Not Over Yet. An Overview of the Current Literature. *J Neurol Surg A Cent Eur Neurosurg* **81**, 64-70, doi:10.1055/s-0039-1688911 (2020).

4 Brennan, C. W. *et al.* The somatic genomic landscape of glioblastoma. *Cell* **155**, 462-477, doi:10.1016/j.cell.2013.09.034 (2013).

5 Network, T. C. Corrigendum: Comprehensive genomic characterization defines human glioblastoma genes and core pathways. *Nature* **494**, 506, doi:10.1038/nature11903 (2013).

6 Wu, F. *et al.* Molecular classification of IDH-mutant glioblastomas based on gene expression profiles. *Carcinogenesis*, doi:10.1093/carcin/bgz032 (2019).

7 Bagley, S. J. & O'Rourke, D. M. Clinical investigation of CAR T cells for solid tumors: Lessons learned and future directions. *Pharmacol Ther*, 107419, doi:10.1016/j.pharmthera.2019.107419 (2019).

8 Romani, M., Pistillo, M. P., Carosio, R., Morabito, A. & Banelli, B. Immune Checkpoints and Innovative Therapies in Glioblastoma. *Frontiers in oncology* **8**, 464, doi:10.3389/fonc.2018.00464 (2018).

9 Alifieris, C. & Trafalis, D. T. Glioblastoma multiforme: Pathogenesis and treatment. *Pharmacol Ther* **152**, 63-82, doi:10.1016/j.pharmthera.2015.05.005 (2015).

10 Perry, A. & Wesseling, P. Histologic classification of gliomas. *Handb Clin Neurol* **134**, 71-95, doi:10.1016/B978-0-12-802997-8.00005-0 (2016).

11 Rulseh, A. M. & Vymazal, J. Whole brain apparent diffusion coefficient measurements correlate with survival in glioblastoma patients. *Journal of neuro-oncology* **146**, 157-162, doi:10.1007/s11060-019-03357-y (2020).

12 Biasibetti, E. *et al.* Comparison of Allogeneic and Syngeneic Rat Glioma Models by Using MRI and Histopathologic Evaluation. *Comp Med* **67**, 147-156 (2017).

13 Harder, B. G. *et al.* Developments in Blood-Brain Barrier Penetrance and Drug Repurposing for Improved Treatment of Glioblastoma. *Frontiers in oncology* **8**, 462, doi:10.3389/fonc.2018.00462 (2018).

14 Ostermann, S. *et al.* Plasma and cerebrospinal fluid population pharmacokinetics of temozolomide in malignant glioma patients. *Clin Cancer Res* **10**, 3728-3736, doi:10.1158/1078-0432.CCR-03-0807 (2004).

15 Vilar, S., Chakrabarti, M. & Costanzi, S. Prediction of passive blood-brain partitioning: Straightforward and effective classification models based on in silico derived physicochemical descriptors. *J Mol Graph Model* **28**, 899-903, doi:10.1016/j.jmgm.2010.03.010 (2010).

16 Kitange, G. J. *et al.* Induction of MGMT expression is associated with temozolomide resistance in glioblastoma xenografts. *Neuro Oncol* **11**, 281-291, doi:10.1215/15228517-2008-090 (2009).
17 Gao, L. *et al.* Suppression of glioblastoma by a drug cocktail reprogramming tumor cells into neuronal like cells. *Sci Rep* **9**, 3462, doi:10.1038/s41598-019-39852-5 (2019).
18 Lu, G. *et al.* Triple-drug Therapy With Bevacizumab, Irinotecan, and Temozolomide Plus Tumor Treating Fields for Recurrent Glioblastoma: A Retrospective Study. *Front Neurol* **10**, 42, doi:10.3389/fneur.2019.00042 (2019).
19 Maraka, S. *et al.* Phase 1 lead-in to a phase 2 factorial study of temozolomide plus memantine, mefloquine, and metformin as postradiation adjuvant therapy for newly diagnosed glioblastoma. *Cancer* **125**, 424-433, doi:10.1002/cncr.31811 (2019).
20 Drukala, J. *et al.* ROS accumulation and IGF-IR inhibition contribute to fenofibrate/PPARalpha -mediated inhibition of glioma cell motility in vitro. *Mol Cancer* **9**, 159, doi:1476-4598-9-159 [pii]
10.1186/1476-4598-9-159 (2010).
21 Grabacka, M. M. *et al.* Fenofibrate Induces Ketone Body Production in Melanoma and Glioblastoma Cells. *Frontiers in endocrinology* **7**, 5, doi:10.3389/fendo.2016.00005 (2016).
22 Koltai, T. Fenofibrate in cancer:mechanisms involved in anticancer activity. *F1000Research* **4**, 1-22, doi:10.12688/f1000research.6153.1 (2015).
23 Wybieralska, E. *et al.* Fenofibrate attenuates contact-stimulated cell motility and gap junctional coupling in DU-145 human prostate cancer cell populations. *Oncol Rep* **26**, 447-453, doi:10.3892/or.2011.1321 (2011).
24 Wilk, A. *et al.* Molecular Mechanisms of Fenofibrate-Induced Metabolic Catastrophe and Glioblastoma Cell Death. *Molecular and cellular biology*, doi:10.1128/MCB.00562-14 (2014).
25 Grabacka, M. *et al.* Fenofibrate subcellular distribution as a rationale for the intracranial delivery through biodegradable carrier. *Journal of physiology and pharmacology : an official journal of the Polish Physiological Society* **66**, 233-247 (2015).
26 Stalinska, J. *et al.* Chemically Modified Variants of Fenofibrate with Antiglioblastoma Potential. *Transl Oncol* **12**, 895-907, doi:10.1016/j.tranon.2019.04.006 (2019).
27 Abotaleb, M. *et al.* Flavonoids in Cancer and Apoptosis. *Cancers* **11**, doi:10.3390/cancers11010028 (2018).
28 Doan, P. *et al.* Alkylaminophenol Induces G1/S Phase Cell Cycle Arrest in Glioblastoma Cells Through p53 and Cyclin-Dependent Kinase Signaling Pathway. *Front Pharmacol* **10**, 330, doi:10.3389/fphar.2019.00330 (2019).
29 Rao, S., Chinkwo, K., Santhakumar, A., Johnson, S. & Blanchard, C. Apoptosis Induction Pathway in Human Colorectal Cancer Cell Line SW480 Exposed to Cereal Phenolic Extracts. *Molecules* **24**, doi:10.3390/molecules24132465 (2019).
30 Romanos-Nanclares, A. *et al.* Phenolic Acid Subclasses, Individual Compounds, and Breast Cancer Risk in a Mediterranean Cohort: The SUN Project. *J Acad Nutr Diet*, doi:10.1016/j.jand.2019.11.007 (2020).

31 Stalinska, J. *et al.* Exploring anticancer activity of structurally modified benzylphenoxyacetamide (BPA); I: Synthesis strategies and computational analyses of substituted BPA variants with high anti-glioblastoma potential. *Sci Rep* **9**, 17021, doi:10.1038/s41598-019-53207-0 (2019).
32 Prinz, H. How to identify a pharmacophore. *Chem Biol* **15**, 207-208, doi:10.1016/j.chembiol.2008.02.013 (2008).
33 Zeslawska, E. *et al.* Pharmacophoric features for a very potent 5-spirofluorenehydantoin inhibitor of cancer efflux pump ABCB1, based on X-ray analysis. *Chem Biol Drug Des* **93**, 844-853, doi:10.1111/cbdd.13473 (2019).
34 Dzialo, M. *et al.* The Potential of Plant Phenolics in Prevention and Therapy of Skin Disorders. *Int J Mol Sci* **17**, 160, doi:10.3390/ijms17020160 (2016).
35 Brown, D. G. & Bostrom, J. Analysis of Past and Present Synthetic Methodologies on Medicinal Chemistry: Where Have All the New Reactions Gone? *J Med Chem* **59**, 4443-4458, doi:10.1021/acs.jmedchem.5b01409 (2016).
36 Pattabiraman, V. R. & Bode, J. W. Rethinking amide bond synthesis. *Nature* **480**, 471-479, doi:10.1038/nature10702 (2011).
37 Dunetz, J. R., Magano, J. & Weisenburger, G. A. Large-Scale Applications of Amide Coupling Reagents for the Synthesis of Pharmaceuticals. *Org Process Res Dev* **20**, 140-177, doi:10.1021/op500305s (2016).
38 Greenberg, J. A. & Sammakia, T. The Conversion of tert-Butyl Esters to Acid Chlorides Using Thionyl Chloride. *J Org Chem* **82**, 3245-3251, doi:10.1021/acs.joc.6b02931 (2017).
39 Rani, P., Pal, D., Hegde, R. R. & Hashim, S. R. Anticancer, Anti-Inflammatory, and Analgesic Activities of Synthesized 2-(Substituted phenoxy) Acetamide Derivatives. *Biomed Res Int*, doi:Artn 386473
10.1155/2014/386473 (2014).
40 Wager, T. T., Hou, X. J., Verhoest, P. R. & Villalobos, A. Moving beyond Rules: The Development of a Central Nervous System Multiparameter Optimization (CNS MPO) Approach To Enable Alignment of Druglike Properties. *Acs Chem Neurosci* **1**, 435-449, doi:10.1021/cn100008c (2010).
41 Wager, T. T., Hou, X. J., Verhoest, P. R. & Villalobos, A. Central Nervous System Multiparameter Optimization Desirability: Application in Drug Discovery. *Acs Chem Neurosci* **7**, 767-775, doi:10.1021/acschemneuro.6b00029 (2016).
42 Rankovic, Z. CNS Drug Design: Balancing Physicochemical Properties for Optimal Brain Exposure. *J Med Chem* **58**, 2584-2608, doi:10.1021/jm501535r (2015).
43 Wu, Z. Y. *et al.* Comparison of prediction models for blood brain barrier permeability and analysis of the molecular descriptors. *Pharmazie* **67**, 628-634 (2012).
44 Wang, J. M. *et al.* Development of Polarizable Models for Molecular Mechanical Calculations I: Parameterization of Atomic Polarizability. *J Phys Chem B* **115**, 3091-3099, doi:10.1021/jp112133g (2011).
45 Naef, R. A Generally Applicable Computer Algorithm Based on the Group Additivity Method for the Calculation of Seven Molecular Descriptors: Heat of Combustion, LogPO/W, LogS, Refractivity, Polarizability, Toxicity and LogBB of

Organic Compounds; Scope and Limits of Applicability. *Molecules* **20**, 18279-18351, doi:10.3390/molecules201018279 (2015).
46 Cha, H. J., Muller, R. T. & Pos, K. M. Switch-Loop Flexibility Affects Transport of Large Drugs by the Promiscuous AcrB Multidrug Efflux Transporter. *Antimicrob Agents Ch* **58**, 4767-4772, doi:10.1128/Aac.02733-13 (2014).
47 Savjani, K. T., Gajjar, A. K. & Savjani, J. K. Drug solubility: importance and enhancement techniques. *ISRN Pharm* **2012**, 195727, doi:10.5402/2012/195727 (2012).
48 Piiper, J. & Worth, H. Value and limits of Graham's law for prediction of diffusivities of gases in gas mixtures. *Respir Physiol* **41**, 233-240 (1980).
49 Stone, N. L., England, T. J. & O'Sullivan, S. E. A Novel Transwell Blood Brain Barrier Model Using Primary Human Cells. *Front Cell Neurosci* **13**, 230, doi:10.3389/fncel.2019.00230 (2019).
50 Srinivasan, B. *et al.* TEER measurement techniques for in vitro barrier model systems. *J Lab Autom* **20**, 107-126, doi:10.1177/2211068214561025 (2015).
51 Garberg, P. *et al.* In vitro models for the blood-brain barrier. *Toxicol In Vitro* **19**, 299-334, doi:10.1016/j.tiv.2004.06.011 (2005).
52 Wang, Y. *et al.* An experimentally validated approach to calculate the blood-brain barrier permeability of small molecules. *Sci Rep* **9**, 6117, doi:10.1038/s41598-019-42272-0 (2019).
53 Dahan, A. & Miller, J. M. The solubility-permeability interplay and its implications in formulation design and development for poorly soluble drugs. *AAPS J* **14**, 244-251, doi:10.1208/s12248-012-9337-6 (2012).
54 An, F. Q. *et al.* Long-term-infected telomerase-immortalized endothelial cells: a model for Kaposi's sarcoma-associated herpesvirus latency in vitro and in vivo. *J Virol* **80**, 4833-4846, doi:10.1128/JVI.80.10.4833-4846.2006 (2006).

ACKNOWLEDGEMENTS: This work was supported by P20-GM121288-01 (KR) and matching funds from the Dean, School of Medicine, LSU Health Sciences Center (KR). All chemistry and computational studies were supported by STEPFARM, LLC. (BSJ).

AUTHOR INFORMATION

Joanna Stalinska, MS
Neurological Cancer Research, Stanley S. Scott Cancer Center, Department of Interdisciplinary Oncology, LSU Health Sciences Center, New Orleans, LA 70112; and Department of Cell Biology, Faculty of Biochemistry, Biophysics and Biotechnology, Jagiellonian University, Cracow Poland.
Charles H. Ingraham IV
Neurological Cancer Research, Stanley S. Scott Cancer Center, Department of Interdisciplinary Oncology, LSU Health Sciences Center, New Orleans, LA 70112D
Sean C. Carson. MS
Department of Chemistry, University of New Orleans, New Orleans, LA 70148, United States.
Cecilia Vittori, MS
Neurological Cancer Research, Stanley S. Scott Cancer Center, Department of Interdisciplinary Oncology, LSU Health Sciences Center, New Orleans, LA 70112; and Department of Biomedical and Clinical Sciences L. Sacco, University of Milan, Milan, Italy.
Adam Lassak, PhD
Neurological Cancer Research, Stanley S. Scott Cancer Center, Department of Interdisciplinary Oncology, LSU Health Sciences Center, New Orleans, LA 70112
Karlie Bonstaff, PhD
Neurological Cancer Research, Stanley S. Scott Cancer Center, Department of Interdisciplinary Oncology, LSU Health Sciences Center, New Orleans, LA 70112
Celeste Faia, PhD student
Neurological Cancer Research, Stanley S. Scott Cancer Center, Department of Interdisciplinary Oncology, LSU Health Sciences Center, New Orleans, LA 70112
Francesca Peruzzi, PhD
Neurological Cancer Research, Stanley S. Scott Cancer Center, Department of Interdisciplinary Oncology, LSU Health Sciences Center, New Orleans, LA 70112
Susan Colley, MS
Grants and Development Office, Stanley S. Scott Cancer Center, LSU Health Sciences Center, New Orleans, LA 70112.

Corresponding Authors

Krzysztof Reiss, PhD
Neurological Cancer Research, Stanley S. Scott Cancer Center, Department of Interdisciplinary Oncology, LSU Health Sciences Center, New Orleans, LA 70112; email: kreiss@lsuhsc.edu; tel: 504 210 2977.
and
Branko S. Jursic, PhD

Department of Chemistry, University of New Orleans, New Orleans, LA 70148, United States and Stepharm llc., PO Box 24220, New Orleans, LA 70184, United States; email: bjursic1@uno.edu, tel: 504 858 0515

Contributions:

JS: performed and help in design of cell culture analyses, cell toxicity tests, microscopy, imaging, data analyses and preparation of the corresponding figures; **CV:** assisted JS in cell culture and toxicity experiments; **KR:** helped designing cell culture experiments, authored manuscript sections related to glioblastoma, cell culture, cell toxicity, and interpretation of the *in vitro* studies; **BSJ:** designed chemical strategies for the development of new HR compounds, performed corresponding chemical reactions, computational analyses of the new compounds, authored the section of the manuscript related to development of chemical modifications and computational analyses; **AL and KB:** performed in vitro BBB penetration assay and HPLC analyses. **CF and FP:** designed and performed experiments and analyzed the data for all metabolic studies of glioblastoma cells treated with HR compounds. **ChI and SCC:** participated in performing specific chemical reactions designed by BSJ, and performed IC50 analyses for some of the HR compounds; **SC:** editing and conceptual effort related to the final design of the manuscript. All Authors reviewed the manuscript.

Competing Interests

Disclosure of Potential Conflict of Interest: Dr. Branko Jursic is associated with Stepharm LLC, P.O. Box 24220, New Orleans, LA; Dr. Reiss is associated with WayPath Pharma LLC. 217 Sena Dr. Metairie LA 70005. Dr. Krzysztof Reiss and Dr. Branko Jursic have an LSU patent for the HR compounds presented in this manuscript ("Anticancer Composition and methods of use" 2932719-056-us2). Other authors do not have any competing interest in relation to this submission.

SUPPLEMENTARY INFORMATION

NMR and MS spectra for all HR compounds generated in this study are included in Supplementary Materials.

Supplementary Files

This is a list of supplementary files associated with this preprint. Click to download.

- SupplementaryMaterials091521.pdf